# Fiber Seismic Network on the Moon

Wenbo Wu<sup>\*1,2</sup>, Zhongwen Zhan<sup>1</sup>, Mark Panning<sup>3</sup>, and Andrew Klesh<sup>3</sup>

#### **Abstract**

Internal structures of the Moon are key to understanding the origin and evolution of the Earth-Moon system and other planets. The Apollo Passive Seismic Experiment detected thousands of lunar seismic events and vastly improved our understanding of the Moon's interior. However, some critical questions like the state and composition of the core remain unsolved largely due to the sparsity of the Apollo seismic stations and the strong scattering of seismic waves in the top layer of the Moon. In this study, we propose the concept of a fiber seismic network on the Moon and discuss its potential in overcoming the challenges in imaging deep Moon structures. As an emerging technique, distributed acoustic sensing (DAS) can provide a cost-efficient solution for largeaperture and dense seismic network deployment in harsh environments. We compute lunar synthetic seismograms and evaluate the performance of DAS arrays of different configurations in retrieving the hidden core reflected seismic phase ScS from the strong scattered waves. We find that, compared to a sparse conventional seismic network, a fiber seismic network using tens of kilometers of cable can dramatically increase the chance of observing clear ScS by array stacking. Our results indicate that DAS could provide new opportunities for the future lunar seismic surveys, but more efforts and further evaluations are required to develop a space-proof DAS.

**Cite this article as** Wu, W., Z. Zhan, M. Panning, and A. Klesh (2024). Fiber Seismic Network on the Moon, *Seismol. Res. Lett.* **95**, 2153–2163, doi: 10.1785/0220230067.

**Supplemental Material** 

#### Introduction

Internal structures of other terrestrial planets (i.e., Mercury, Venus, and Mars) and the Moon are key to our understanding of their and the Earth's thermochemical states, origins, and evolutions in comparative planetology. The Moon is of particular interest, due to not only its close distance to the Earth, which makes a space mission much easier, but also because the scientific questions of its origin, evolution, and mechanical behaviors are closely tied to those of the Earth (Canup and Asphaug, 2001). Much of our present knowledge about the Moon's interior comes from geophysical investigations, including seismic, gravity, heat flow, magnetic, and ground-penetrating radar surveys in the last few decades (Hood, 1986; Wieczorek et al., 2006; Garcia et al., 2019). Of these methods, seismic waves can penetrate the deep Moon and therefore help us reveal a rather detailed structure (e.g., Nakamura, 1983; Lognonné et al., 2003; Gagnepain-Beyneix et al., 2006; Garcia et al., 2011; Weber et al., 2011; Khan et al., 2014; Matsumoto et al., 2015). As a pioneering planetary seismic exploration program, four seismometers were deployed on the Moon during the Apollo missions (12, 14, 15, and 16) in 1969-1976, and provided the unique data to investigate the Moon seismic activities and structures (Fig. 1; Latham et al., 1970; Nakamura et al., 1982).

During the seven years of operation, the Apollo seismometers detected thousands of seismic events from the near side of the Moon, which can be generally classified to four groups: shallow moonquakes, meteorite impacts, artificial impacts, and deep moonquakes (Toksöz *et al.*, 1974; Lammlein, 1977; Nakamura, 1983; Nunn *et al.*, 2020). Most of these moonquakes have very small magnitudes (e.g., M < 3, Goins *et al.*, 1981) but have been recorded in high quality, benefiting from the extremely quiet seismic environment and low attenuation on the Moon, as well as the high sensitivity of the Apollo seismometers (Latham *et al.*, 1970).

Based on the Apollo seismic data, several 1D models of lunar interior structure have been developed (e.g., Nakamura, 1983; Lognonné et al., 2003; Gagnepain-Beyneix et al., 2006; Garcia et al., 2011; Weber et al., 2011; Khan et al., 2014; Matsumoto et al., 2015), but large uncertainties are still present, especially about the core. The most prominent feature of the moonquake seismograms is the emergent first arrival with a long duration of coda waves (Fig. 2; Nakamura, 1977; Nunn et al., 2020), which is distinct from the relatively impulsive signals from earthquakes. This feature is also seen on the marsquake seismograms (Banerdt et al., 2020), and attributed to the strong scattering effects in the top porous regolith and crustal fractures created

<sup>1.</sup> Division of Geological and Planetary Sciences, California Institute of Technology, Pasadena, California, U.S.A., (a) https://orcid.org/0000-0002-6249-8065 (WW); (b) https://orcid.org/0000-0002-5586-2607 (ZZ); 2. Geology and Geophysics Department, Woods Hole Oceanographic Institution, Woods Hole, Massachusetts, U.S.A.; 3. Jet Propulsion Laboratory, California Institute of Technology, Pasadena, California, U.S.A., (b) https://orcid.org/0000-0002-2041-3190 (MP); (b) https://orcid.org/0000-0003-4190-7891 (AK)

<sup>\*</sup>Corresponding author: wenbo.wu@whoi.edu

<sup>©</sup> Seismological Society of America

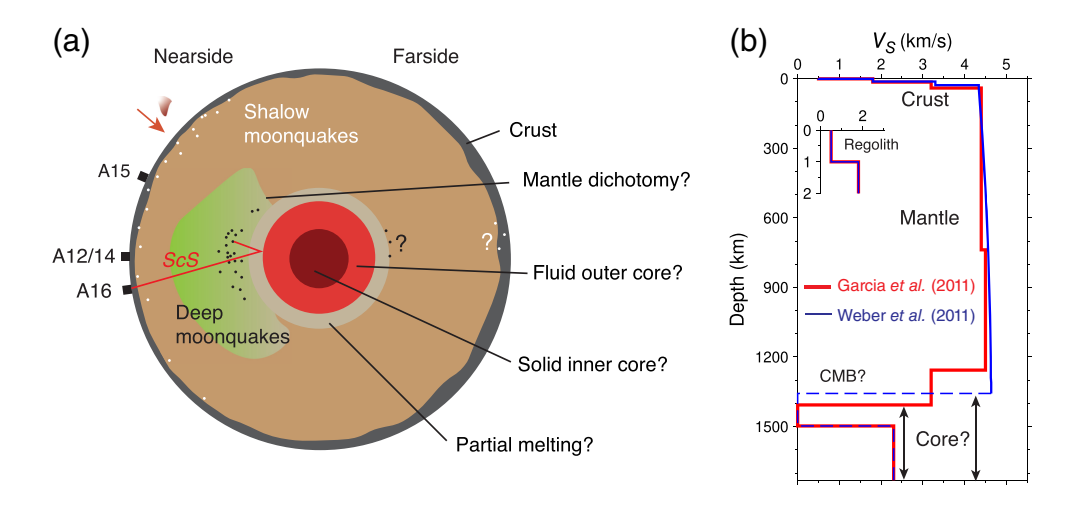


**Figure 1.** Lunar seismicity and the 1D shear velocity models of the Moon. (a) A cartoon of lunar seismicities and interior structures. Modified from Wieczorek *et al.* (2006). The black squares represent the four Apollo seismometers. The black circles illustrate the deep moonquakes detected at the near side and their questionable presence at the far side. The white circles are shallow moonquakes, and the red arrow indicates a meteorite impact. The red line shows the path of core phase *ScS.* (b) Two depth profiles of shear velocity of the Moon proposed by Garcia *et al.* (2011) (red line) and Weber *et al.* (2011) (blue line). "?" indicates that the existence of these moon structure's properties is uncertain with our community's current understanding. The color version of this figure is available only in the electronic edition.

by impactors (Dainty *et al.*, 1974; Blanchette-Guertin *et al.*, 2012; Gillet *et al.*, 2017). These scattered waves obscure any later arrival phase, such as the *S* waves and reflected waves from internal

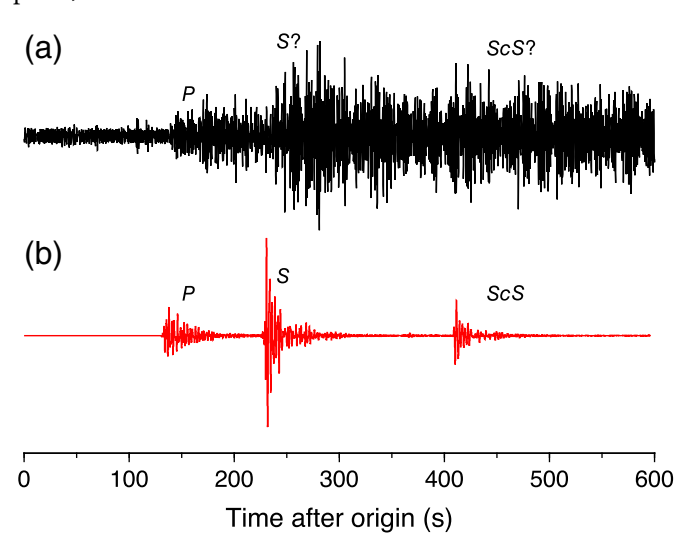


**Figure 2.** (a) Observational data and (b) 1D synthetic seismogram of a deep moonquake. (a) A 0.2–2 Hz filtered horizontal component recorded by long-period sensor at the Apollo station 14 from a deep moonquake within the cluster A1. This moonquake is located at a depth of 918.5 km (Garcia *et al.*, 2011), but a large uncertainty is present. (b) A horizontal component of 1D synthetic seismogram using the 1D velocity model by Garcia *et al.* (2011), which does not replicate the strong scattered coda of the observed data. "?" means that the signal ScS should arrive at that time, but we cannot clearly identify it due to the contaminating signals. The color version of this figure is available only in the electronic edition.

discontinuities (e.g., core-mantle boundary reflected phases PcP and ScS), therefore result in large uncertainties in moonquake locations and deep Moon structures (Weber et al., 2011). The recent efforts in combining multiple geophysical constraints and developing new methods to reanalyze the Apollo seismic data have enabled scientists to partially overcome the difficulties caused by contaminating coda waves and sparse stations (see Garcia et al., 2019). For example, Wieczorek et al. (2013) combined the high spatial resolution of GRAIL gravity data with other constraints including Apollo seismic data, and revealed a more detailed distribution of the lunar crust thickness and porosity. Weber et al. (2011) applied polarization

filtering on the data from deep moonquakes, and provided a new estimate of the size and state of the core.

The Apollo seismic data provided important insight into the lunar mechanical properties and interior structures. However, many outstanding scientific questions of lunar seismology remain unsolved. For example, some shallow moonquakes might be associated with the Moon tectonics (Watters et al., 2019), but why do deep moonquakes occur at the depths of 700-1100 km (Fig. 1), where ductile deformation, instead of brittle failures, is expected (Toksöz et al., 1977; Cheng and Toksöz, 1988; Koyama and Nakamura, 1980; Frohlich and Nakamura, 2009)? What is the reason for the lack of detected moonquakes from the Moon far side (Nakamura, 2005)? Many puzzling questions regarding lunar structure have also been raised, such as the existence of partially molten lowermost mantle (Nakamura et al., 1973; Nakamura, 2005; Weber et al., 2011; Khan et al., 2014), the existence of dichotomy lunar mantle structure (Qin et al., 2012; Laneuville et al., 2013), and the properties of the core (Yamada et al., 2014; Garcia et al., 2019). Particularly, constraining the structure of core is always one of the top goals in planetary geophysical missions, due to the important role of the core playing in planetary evolution, geodynamo, and habitability. Although the Apollo data provided some hints on the status of the core (Weber, 2011; Garcia et al., 2011), studies about its size and properties are still inconclusive (Fig. 1b, Yamada et al., 2014; Garcia et al., 2019).

Answering these questions requires more seismometers (Nunn *et al.*, 2020), preferably dense seismic arrays, to form a network and reduce the contamination effects of scattered waves.

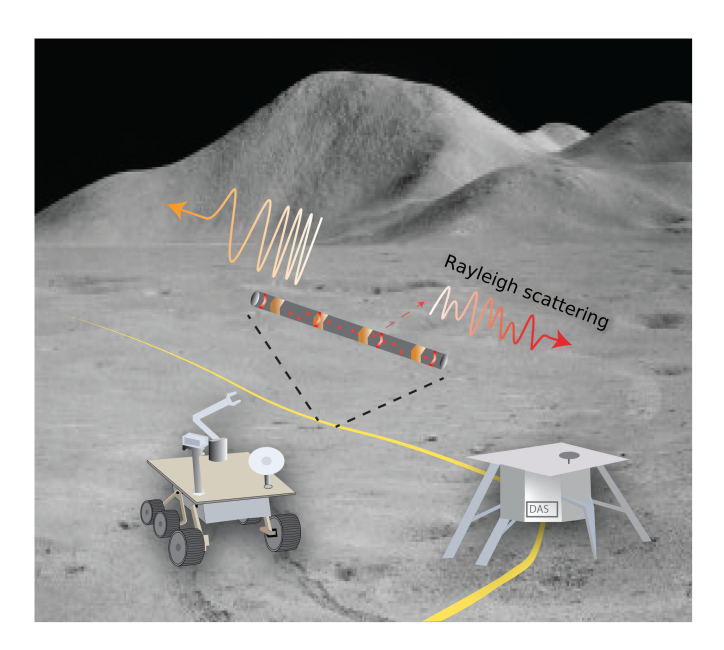


Figure 3. A conceptual lunar fiber seismic network (background lunar surface image from National Aeronautics and Space Administration [NASA]). The base station provides space and power for the distributed acoustic sensing (DAS) interrogator, data processing unit, and telecommunicating system. The cables (yellow belt) can be deployed by a lunar rover. DAS uses the Rayleigh backscattered light by intrinsic fiber defects (red dots in the enlarged cable section) to detect the longitudinal strain. The color version of this figure is available only in the electronic edition.

Constrained by the high cost, planetary seismology has mostly been focusing on deployments of single device (e.g., Mars InSight; Banerdt et al., 2020; Lognonné et al. 2019, 2020) or a few stations (e.g., Apollo seismometers). As an emerging technique, distributed acoustic sensing (DAS) provides a scalable solution for dense array deployment with a relatively low cost and has demonstrated a wide range of successes on the Earth (see recent reviews by Zhan, 2020 and Lindsey and Martin, 2021). In this study, we conduct synthetic tests and explore the potential of a fiber seismic network deployed on the Moon for better lunar structure imaging, particularly recovering the core phase within the strongly scattered waves.

## **Potential Applications of Fiber Seismic Network on the Moon**

DAS can turn every few meters of a tens of kilometers long optical fiber into a seismic sensor by attaching an interrogation unit to one end of the fiber (Zhan, 2020). DAS works by shining a laser pulse into the fiber from one end and interrogating the "echo" of Rayleigh scattering from intrinsic fiber defects (Fig. 3). If a fiber section is strained, the relative positions of the fiber defects within the section will change, and so will the corresponding backscattering in both amplitude and phase. DAS measures the changes at a high sampling rate (e.g., 10 kHz) and converts them to strain measurements.

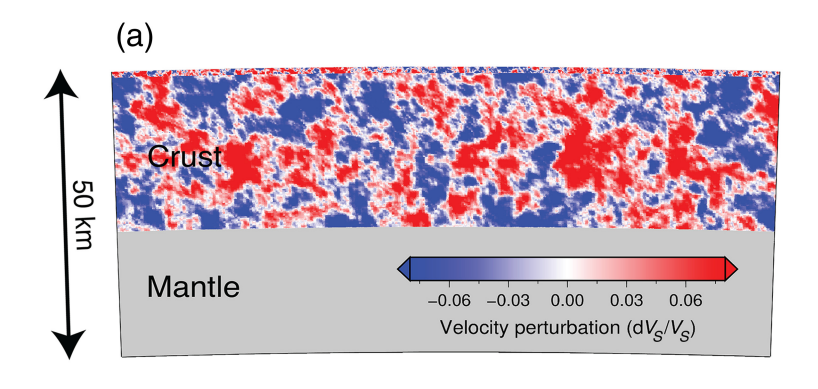
Applications of DAS on seismic imaging, earthquake source studies, and seismic hazard assessment have been well demonstrated in a number of field experiments on the Earth (see compilation in Lindsey and Martin, 2021). It turns out that almost all of the mature seismic imaging methods developed for conventional seismometers can be transferred to DAS data with some necessary adaptations. For example, DAS data with small array spacing are suitable for high-resolution subsurface structure imaging based on either passive or manmade sources. Reports of teleseismic waves are fewer, but the preliminary study by Yu et al. (2019) shows promising results of surface-wave dispersion measurement and receiver function constraints on crust structure. Combining the array stacking and template matching method, DAS shows comparable or even better performance of detecting small earthquakes than conventional network (Li et al., 2021). Another advantage of DAS is its relatively simple procedure of deployment and strong survival capability under harsh conditions. Thus, DAS would be much favored in the regions with harsh environments (Lindsey et al., 2019; Sladen et al., 2019; Williams et al., 2019; Walter et al., 2020), in which conventional electronic seismic sensors are costly and less sustainable due to the limited power supply.

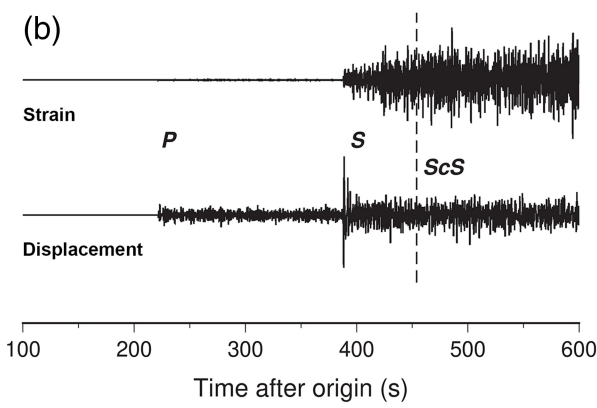
The successful applications of DAS on the Earth inspire the idea of deploying a fiber seismic network on the Moon, which may help us overcome some of the difficulties that the sparse Apollo stations had. The first goal of such a fiber network is to detect as many lunar seismic events as possible. Although the experiments on the Earth show great capability of detecting small earthquakes, seismic signals from moonquakes are much weaker and demand high sensitivity of any lunar seismometer. In addition, the harsh environments on the Moon are another common challenge of designing a planetary seismometer. Fibersensing cables could be engineered to survive harsh lunar environments more easily than individual sensors with sensitive electronics. Solving these two problems needs efforts from scientific and engineering communities, and we leave some more detailed discussions to the last section of this article. In this study, we focus more on the scientific question of exploring the potential of fiber network on imaging the deep Moon structure. As a specific example, we numerically simulate the wave propagation in a 1D Moon structure model with small-scale heterogeneities present in the crust and investigate the possibility of recovering the core phase ScS—the shear waves reflected at the core-mantle boundary (CMB) from the DAS synthetic data.

## Synthetic Investigation of Retrieving **Lunar Core Phase ScS**

Synthetic method and model setup

Accurate 3D seismic synthetics would be ideal for us to investigate the scattered waves, but it is too computationally expensive. Thus, we use a more computationally efficient tool-AxiSEM (Nissen-Meyer et al., 2014) to compute lunar DAS strain synthetics. AxiSEM assumes an axis-symmetric





spherical body (i.e., 2.5D structure) such that a 3D wave propagation problem can be efficiently solved by a full numerical simulation in a 2D domain and combining it with the analytical solution on the third dimension of azimuth. The 2D wave propagation simulation is computed using the spectral element method, in which many complex structures, such as discontinuity topography, anisotropy and attenuation, can be conveniently incorporated. AxiSEM has been widely used to model seismic wave fields at a global scale on the Earth, including scattered waves in the deep Earth (e.g., Wu and Irving, 2017; Haugland *et al.*, 2018).

The synthetic model used in our study is formed by combining the 1D structure by Garcia et al. (2011) with heterogeneities distributed in the 27 km of crust and the top 1 km of regolith (Fig. 4). We note that discrepancies are present between the 1D models derived from different data and inversion methods (e.g., Nakamura, 1983; Lognonné et al., 2003; Gagnepain-Beyneix et al., 2006; Garcia et al., 2011; Weber et al., 2011; Khan et al., 2014; Matsumoto et al., 2015), especially in the crust and core (Fig. 1). However, the goal of our study is to recover ScS from the scattered waves, and we expect similar conclusions when other 1D models are used. The heterogeneities in the crust are represented by stochastic models generated with an exponential autocorrelation function (ACF) as shown in Figure 4a. The ACF is described by the autocorrelation length, *a*, and root mean square (rms) perturbations of S-wave velocity,  $V_S$ , P-wave velocity,  $V_P$ , and density,  $\rho$ . Other kinds of ACFs, such as Von Karman and Gaussian ACFs, have also been used to describe stochastic models of heterogeneities in the Earth (see chapter 2 of Sato et al., 2012). These ACFs predict different spatial patterns of heterogeneities and therefore cause different frequency dependent effects in seismic wave propagations. Thus, they could be resolved by investigating scattered waves across different frequencies. However, it would be difficult to distinguish them if only a narrow frequency band of data is available, which is the case for Apollo seismic data. In other words, any ACF model can be chosen if only a narrow frequency band is considered (Wu et al., 2019).

The 2D AxiSEM domain is meshed using 14,693 elements to resolve 2 Hz seismic waves. We refine the meshes in the top

**Figure 4.** Heterogeneity model and synthetic seismograms. (a) Heterogeneities in the crust and regolith. The blue–red colors show a stochastic model of  $V_S$  perturbations generated using the exponential autocorrelation function with a=2 km and root mean square (rms) = 6% in the 27 km crust and top 1 km regolith. (b) Normalized displacement and radial strain synthetic seismograms (0.2–2 Hz) corresponding to the heterogeneity model in panel (a). The dashed line indicates the predicted ScS arrival time. ScS is hidden in the scattered waves produced by the heterogeneities. The color version of this figure is available only in the electronic edition.

regolith to match its extremely low seismic velocities (Fig. 4), and the heterogeneities contained in this thin layer are uncorrelated with their counterpart in the underlying crust (Fig. 5). We place a source at a relatively large depth of 900 km, which would produce less scattered waves than that from a shallow moonquake (Blanchette-Guertin et al., 2015). The previous analyses indicate that clustered deep moonquakes may occur on nearly horizontal planar faults (Nakamura, 1978; Koyama and Nakamura, 1980; Wang et al., 2013). Thus, we use a double-couple source focal mechanism with a dip angle of zero degrees. DAS is placed on the azimuth of 180° relative to the fault-slip direction, which produces a radiation pattern with the strongest transverse component ScS. The central location of DAS array is placed at a distance of 75.5°. Because DAS is most sensitive to axial strain, we set the DAS orientation to 45° off the azimuth from the source to the DAS central location to maximize ScS signals. We choose the transverse component ScS, because the complete reflection of ScS at the CMB increases the chance of observing ScS. In other words, the transverse component ScSH plays an important role in detecting a lunar outer core (Garcia et al., 2011; Yamada et al., 2014). In the next subsection, we will compute the strain synthetics of DAS array, and assess its performance with different cable lengths and channel spacings in retrieving ScS, in terms of signal-to-noise ratio (SNR).

#### Retrieving the core phase ScS

In the last decades, stacking techniques based on array seismic data have been widely used to analyze and retrieve weak signals

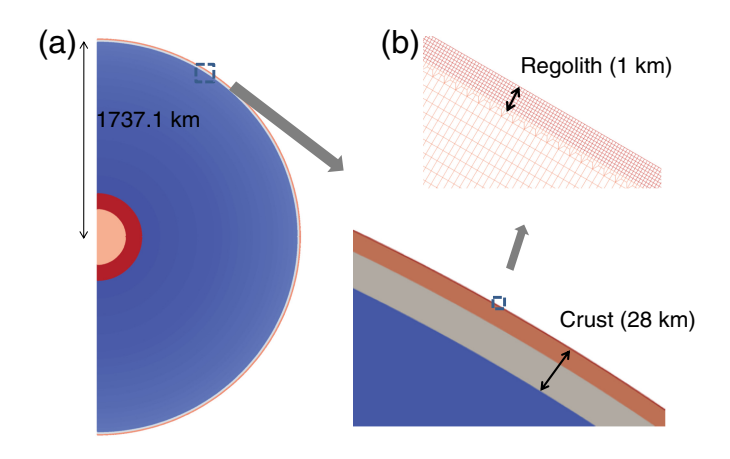


**Figure 5.** The 2D meshes of the Moon used in AxiSEM. (a) The half-circle model shows the layered structure of the Moon, including a solid inner core in the center (pink), a fluid outer (red), a thick mantle (blue), and a thin layer of crust (including the barely visible regolith) at the top (lower crust in gray and upper crust in brown). (b) The 1 km regolith layer is meshed using refined meshes to match its low seismic velocities. The 2.5D structure simulated by AxiSEM is formed by rotating the 2D domain along the vertical symmetrical axis. The color version of this figure is available only in the electronic edition.

from the deep Earth (Rost and Thomas, 2002). In the following, we will apply the simple linear stack method to synthetic seismograms of DAS array for retrieving *ScS* from the scattered waves. At first, we will show the results from the case of relatively weak heterogeneities in the crust. Then, we will discuss the possible ways to improve the SNR of retrieved *ScS* when stronger heterogeneities are present.

The autocorrelation length, a, describes the characteristic scale of heterogeneities and affects how scattering happens at different frequencies. To our knowledge, there has not been any reliable estimation of this parameter for the Moon. Numbers ranging from 1.3 to 9.1 km with the Van Karman ACF have been used in the previous numerical simulations (Yao, 2016; Jiang et al., 2015) but have not been tested by systematically comparing their predictions to observational data. Actually, the trade-off between a and rms perturbations of  $V_S$ ,  $V_P$  and  $\rho$  does not permit tight constraints on these parameters, if only a narrow frequency band of seismic data is available, which is the case of the Apollo data. Thus, we set a to 2 km (Fig. 4), which is close to the wavelength of S wave in the crust for strong scattered wave genesis. The rms perturbations of  $V_P$ ,  $V_S$ , and  $\rho$  are given as  $dV_S/V_S = 6\%$ ,  $dV_P/V_P = 3\%$ , and  $d\rho/\rho = 3\%$ , respectively. Similar as the observed data, these heterogeneities produce scattered waves, which obscure the late arrival phase ScS (Figs. 2 and 4b).

We incorporate the heterogeneities in AxiSEM, simulate the axial strain synthetics of DAS, and filter them to 0.5–1.0 Hz. The spacing of DAS channels is specified as 0.1 km, which is much shorter than the *S* wave wavelength in the low-velocity

regolith layer. Similar to the Apollo data, the scattered waves produced by the heterogeneities dominate the seismograms, and ScS is hidden (Fig. 6a,c). To retrieve ScS, we apply the linear stack to the synthetics for suppressing the less coherent and slower scattered waves across DAS channels. To demonstrate the role of cable length, we design experiments with two different lengths of 20 km (Fig. 6a,b) and 80 km (Fig. 6c,d), which are composed of 200 and 800 individual channels, respectively. In the 80 km long case, we successfully retrieve ScS signal (Fig. 6c) at its expected arrival time and apparent velocity of 26.36 km/s (Fig. 6d). In contrast, the length of 20 km is too short to effectively reduce the energy of scattered waves, so ScS is still invisible on the stacked seismogram (Fig. 6a). In both the cases, we can see ubiquitous inclined stripes with high amplitudes in the synthetic profiles (Fig. 6a,c), and these waves correspond to the high-energy part with apparent velocities of 0.5–4 km/s in Figure 6b,d. We attribute them to the scattered waves trapped in the crust and regolith, which explains their apparent velocities close to the background shear velocities in the crust and regolith (Fig. 1b). The dramatically different apparent velocities between ScS and scattered waves allow us to separate them from each other.

The SNR of retrieved ScS depends on not only the cable length but also the spacing of array elements. As Figure 7 shows, successfully retrieving ScS relies on a sufficiently long cable and an adequate number of channels. For this particular model of heterogeneities, a 40 km or longer cable with a 0.1 km or smaller channel spacing would give us a good chance to retrieve ScS with SNR > 2.0. The SNR is defined as the peak-to-peak amplitude ratios of ScS to noise. The ScS amplitude is measured in a time window between 5 s before and 10 s after the ScS arrival time predicted using the 1D model by Garcia et al. (2011). The time window of noise is taken from 25 to 5 s before the ScS arrival time. A longer cable length generally increases the SNR of retrieved ScS as long as the travel-time anomalies of ScS due to heterogeneities are not too large to affect coherent stacking of ScS. Given a fixed cable length, increasing the number of array elements is also helpful. However, it reaches a saturated SNR when the spacing gets much smaller than the wavelength, because waveforms between consecutive channels become almost identical, and adding more interpolated channels just provides redundant seismograms. As Figure 7a shows, this saturation happens at a channel spacing of roughly 0.1 km, which is much larger than the common DAS channel spacing of ~1-10 m. In other words, a great advantage of DAS data is the superior intersensor spacing, which permits high-quality array analysis of seismic waves with frequencies up to tens of Hertz.

We note that *ScS* is usually observed at relatively low frequencies (i.e., <0.2 Hz) on the Earth, because their high-frequency components dramatically decay due to the high attenuation. For the Moon, the intrinsic attenuation is much weaker than that in the Earth (Nakamura and Koyama, 1982; Blanchette-Guertin *et al.*, 2012; Gillet *et al.*, 2017), which is

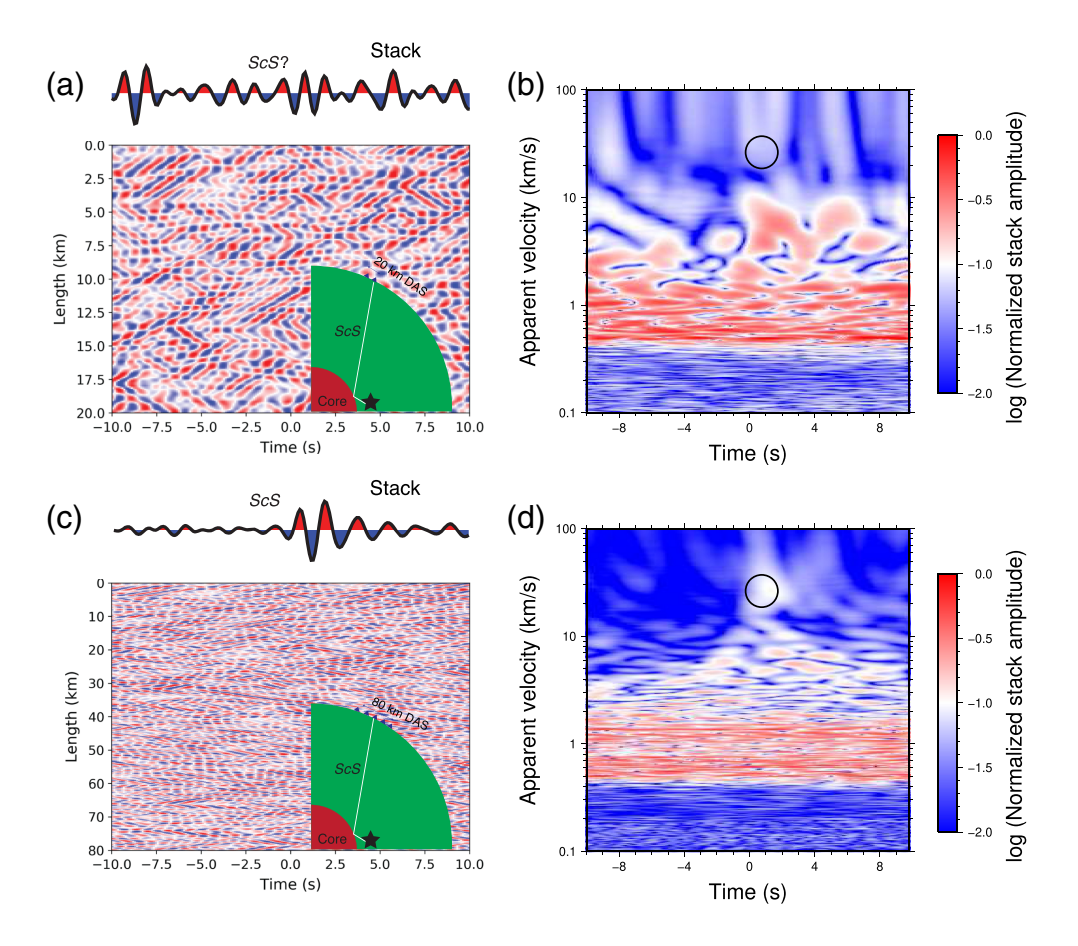


**Figure 6.** Array analysis of DAS synthetics at 0.5–1 Hz. The corresponding model of heterogeneities has an autocorrelation length of 2 km and rms perturbations of  $dV_5/V_5 = 6\%$ ,  $dV_P/V_P = 3\%$ , and dP/P = 3%. (a) A 20 km long DAS synthetic profile (bottom) and its stacked seismogram (top). The stacked seismogram is obtained by shifting and stacking waveforms of each channel using an apparent velocity of 26.36 km/s. The inset cartoon shows the source (black star), DAS sensors (blue triangles), and a ray path of ScS. Time zero is the arrival time of ScS predicted using the 1D model by Garcia et al. (2011). Note that DAS sensors follow an orientation of 45° off the source—receiver azimuth, but they are simply projected to this 2D plane for visualization convenience. (b) Array analysis of DAS synthetics in panel (a). The black circle marks the expected ScS arrival time and its apparent velocity of 26.36 km/s according to the 1D model by Garcia et al. (2011). (c,d) The same as panels (a) and (b) but for a 80 km long DAS array. "?" indicates the signal ScS is weak, and we can see some energy, but it is contaminated by noises. The color version of this figure is available only in the electronic edition.

supported by the stronger *S* wave than *P* wave even at short periods (Fig. 1). Thus, observing lunar *ScS* across a wide frequency band is possible, and its frequency-dependent features would inform us about more detailed properties of the core mantle boundary, such as sharpness and topography. On the other hand, scattering in the Moon's crust must also has frequency-dependent behaviors that would affect the retrieval of *ScS* at different frequencies. Thus, we also repeat to stack the strain synthetics at another two frequency bands (0.2–0.5 Hz in Fig. S1a, available in the supplemental material to this article, and 1–2 Hz in Fig. S1b) and compare their results to that at 0.5–1 Hz (Fig. 7a). Given the same cable length and channel spacing, the retrieved *ScS* at lower frequencies generally shows higher SNRs. In the readily observable domain (i.e., cable

length larger 40 km and chanspacing smaller than 0.1 km), SNRs are generally higher than 3 at 0.2-0.5 Hz, become weaker but still higher than 2 at 0.5-1 Hz, and drop below 2 at 1-2 Hz. This trend might be caused by multiple factors, including frequencydependent scattering strength and less coherent ScS stacking at higher frequencies. It has been known that scattering intensity or attenuation are maximized when the wavelength is comparable with the autocorrelation length of structure heterogeneities (Sato et al., 2012). Thus, the wavelengths of 0.2–0.5 Hz S wave in the crust are much larger than the specified autocorrelation length of 2 km, and weak scattered waves would be expected that result in higher SNRs. In contrast, the scattering intensity at 1-2 Hz becomes stronger. In addition, the travel-time anomalies due to heterogeneities become comparable with the dominant period of 1-2 Hz waves and therefore cause less coherent ScS stacking. These results indicate that working on lower frequencies would increase the chance of retrieving ScSalthough the instrument sensitivity is another issue, which we will discuss later.

Because of different sensing principles, DAS systems typically measure strain or strain rate when conventional seismometers usually record displacement, velocity, or acceleration of ground motion. To compare their performance in retrieving lunar ScS, we use displacement synthetics, instead of axial strain, for stacking and find dramatically improved SNRs (Fig. S2). For example, a 40 km array composed of 400 conventional sensors can provide us with a SNR up to 10 (Fig. S2), much higher than the SNR of 2–3 from the stacking of axial strain synthetics (Fig. 7a). We propose that the major reason for this is the amplified scattered waves in the axial strain synthetics. Assuming plane-wave incident, the axial strain is inversely proportional to phase velocity (Yu et al., 2019). The coda waves are trapped in the crust and mostly propagate along the horizontal direction,

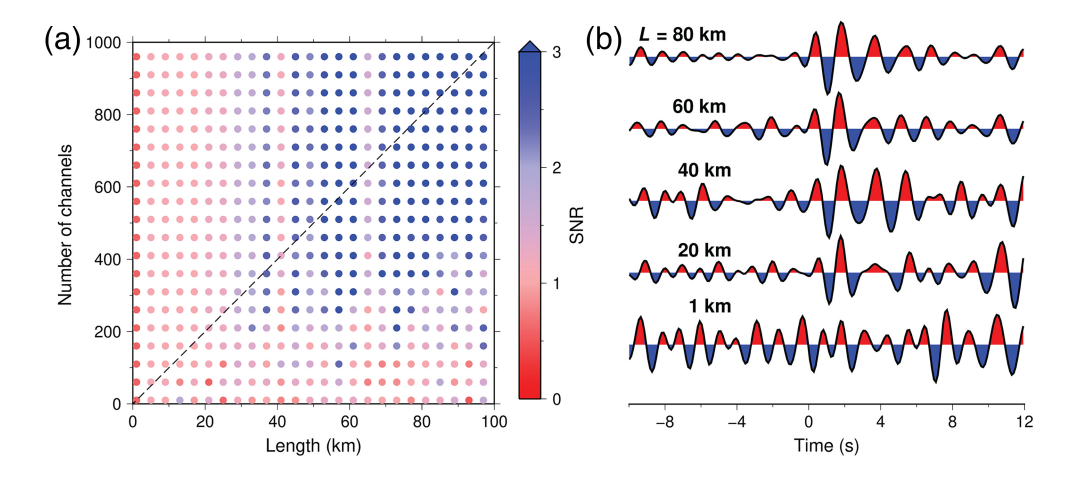


**Figure 7.** Signal-to-noise ratios (SNRs) and stack waveforms of retrieved *ScS* with different cable lengths and channel numbers of DAS array. The heterogeneity model has an autocorrelation length of 2 km and rms perturbations of  $dV_S/V_S=6\%$ ,  $dV_P/V_P=3\%$ , and  $d\rho/\rho=3\%$ . (a) SNRs of retrieved *ScS*. The black dashed line corresponds to a DAS channel spacing of 0.1 km. (b) The stack waveforms of *ScS*. Time zero is the arrival time of *ScS* predicted using the 1D model by Garcia *et al.* (2011). The number above each stacked seismogram represents the length of DAS used. The channel spacing is 0.1 km for all of these stacked seismograms. The color version of this figure is available only in the electronic edition.

so they have almost one order of magnitude lower apparent phase velocities than the more vertically incident ScS (Fig. 6b, d). This dramatic difference amplifies the coda wave by a factor of  $\sim$ 10 on the axial strain (e.g., the stronger S wave in the displacement seismogram than that in the radial strain in Fig. 4b). This amplification makes retrieving ScS using displacement synthetics much easier than that based on strain synthetics. Although typical DAS systems using a simple horizontal optical-fiber cable is only sensitive to the strain along the fiber axis, the recently proposed broadside-sensitive DAS uses more complex fiber geometries (e.g., helical wound) to enhance broadside sensitivities and has the potential to measure the full strain tensor, from which three-component displacement can be derived (Kuvshinov, 2016; Hornman, 2017; Lim Chen Ning and Sava, 2018). This new type of DAS sensing cable would dramatically enhance our capability of detecting ScS and other core phases if deployed on the Moon.

In the earlier simulation, a model of relatively weak heterogeneities is used, whereas the lunar crust and regolith might be more heterogeneous than that (Blanchette-Guertin *et al.*, 2012; Gillet *et al.*, 2017). To test the performance of DAS when stronger scattered waves are present, we regenerate a stochastic model using increased  $V_S$ ,  $V_P$  and density perturbations of 15%, 15%, and 15%, respectively, while keeping the autocorrelation length at 2 km. Consequently, the simulated scattered waves become stronger, which results in a failure of retrieving *ScS* based on the strain synthetics at 0.5–1.0 Hz. In addition, the SNR of retrieved *ScS* also depends on the source focal mechanism and the DAS deployment location. An unfavorable radiation pattern for *ScS* can also lead to low SNR (Fig. S3). To

increase the SNR of stacked ScS, a straightforward solution would be expanding the cable length, but it requires additional costs on mission paydeploying load, and data processing, and on. Another less costly solution would be taking advantage of broadside-sensitive DAS to increase the deep Moon signals in each DAS channel. For example, using 0.2-0.5 Hz broadside-sensitive DAS data with a 20 km or longer cable would allow us to retrieve ScS with SNR > 4 for the strong scattering wave case (Fig. S4). The SNR is low if only a handful of sensors (e.g., conventional seismometers) available, and retrieving clear ScS can only be achieved by

deploying a sufficient number of sensors, for example, broadside-sensitive DAS array.

#### **Discussion and Conclusion**

Dense seismic arrays on the Earth have many unique advantages in detecting small earthquakes, retrieving weak signals from the deep Earth and imaging shallow structures with an unprecedented high resolution. DAS has proved to be a cost-efficient solution for many of these applications by an increasing number of field experiments. In this article, we have discussed the possibility of detecting the core phase ScS by deploying a fiber seismic network on the Moon. Besides deep Moon research, a fiber seismic network could also improve our capability of imaging shallow and deep Moon structures, and recording small lunar seismic activities. For example, stacking array data can reduce any random environmental seismic noises and therefore permits small-magnitude moonquake detections. This detection capability will also be useful for detecting, locating, and characterizing impacts as done with Apollo data (e.g., Oberst and Nakamura, 1991). Without the atmospheric filtering of small impactors, impact studies on the Moon are valuable for looking at impact processes throughout the solar system (e.g., Daubar et al., 2018). Reliable estimations of crustal thickness through receiver functions (Vinnik et al., 2001; Yu et al., 2019) can be jointly inverted with satellite gravity data (Wieczorek et al., 2013), by which the global distribution of crust thickness and porosity can be better mapped out. Imaging shallow structures, such as the top fractured zone, underneath the tens-of-kilometer-long cable would provide us with critical insights into the associated processes of meteorite impactor and magma activities.

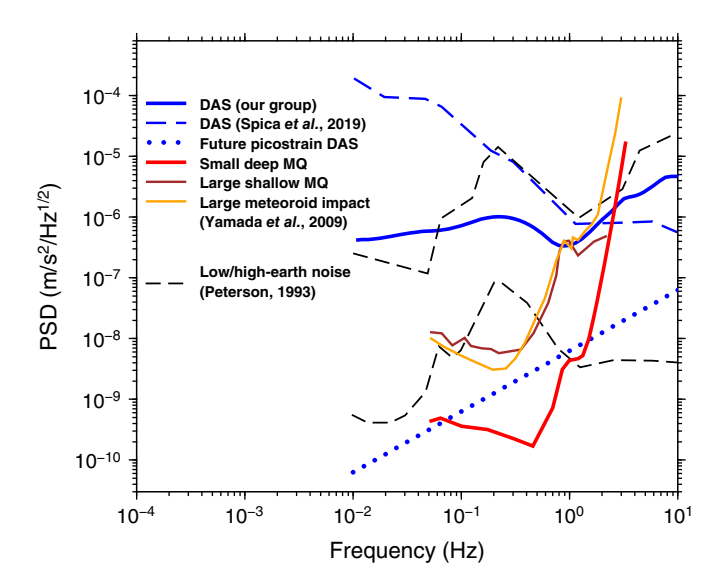


**Figure 8.** Power spectral density (PSD) of signals from seismic activities on the Moon, instrument self-noise, and ambient noises on the Earth. The blue lines show the PSD of signals observed by DAS from two typical field experiments by Spica *et al.* (2020) and our group. The red, brown, and orange lines represent the signals from a deep moonquake, shallow moonquake, and meteoroid impact (Yamada *et al.*, 2009). The two black dashed lines show the new high-noise model (NHNM) and the new low-noise model (NLNM) of the Earth by Peterson (1993). The color version of this figure is available only in the electronic edition.

Achieving these goals requires usage of seismic signals with distinct periods, so it is desired to deploy a fiber network that has high sensitivities to a relatively broad band of frequencies. For example, it would be much easier to retrieve ScS at the low frequencies, while the relatively high-frequency waves would be more useful for imaging shallow structures with high spatial resolution. Different from the Earth, the Moon has a much lower environment noise level and weaker intrinsic seismic attenuation, which helped the Apollo seismometers to record the extremely weak signals from various types of seismic activities (Fig. 8). However, many of these signals were only observed at the high-frequency part (i.e., >0.2 Hz). The corresponding low-frequency signals are higher than environmental noises, but they drop below the instrument sensitivities of Apollo seismometers. Thus, instrument sensitivity is a key factor in designing planetary seismometers. The Apollo seismometers, when quite sensitive, were also limited by coarse digitization (Nunn et al., 2020). However, modern planetary seismic sensors are capable of even greater sensitivity (e.g., the very broadband sensor of InSight, Lognonné et al., 2019), and ongoing development of planetary seismometers focused on lunar operation, such as the micromachined Silicon Seismic Package-lunar (Nunn et al., 2021), are expected to have improved sensitivities, which would enable us to record even weaker signals. Currently, the sensitivities of DAS used in the field experiments on the Earth depend on many factors, including instrument type, environment conditions, and specific installations, so they vary substantially from one experiment to another. However, some typical experiments already show promising results of recording high-frequency seismic signals at >1 Hz, which have comparable power spectral density with that from shallow moonquakes (Fig. 8). Although the instrument noises of current DAS are still high, especially at the low-frequency part, and not qualified for planet missions yet, we expect them to be significantly improved in the future. For example, a large portion of the noise comes from the environment conditions, such as temperature variations, and electronic noises. In contrast to the Earth, the temperature variations on the Moon are extremely weak at short-time scales comparable with periods of seismic waves, even though they vary greatly between lunar day and night. Thus, a fiber seismic network on the Moon may not suffer from this problem as much. In the laboratories, DAS is already able to reach picostrain/Hz sensitivity when these noise factors are well-controlled (Costa et al., 2019; Fig. 8). We expect a future specialized lunar DAS with a similar or even lower noise level, and the signals from small, deep moonquakes would become observable at individual channels of this lunar DAS. Stacking data from all the channels could further reduce the noises and improve SNRs of weak signals. Although optical noise of the DAS laser source causes common-mode noise that can be not canceled by stacking, more stable laser sources should be used for lunar DAS and will reduce the common-mode noise substantially (Araki et al., 2022). Another limitation of current DAS is the reduced strain sensitivity away from the cable axis. Because the scattered waves travel more horizontally with a lower apparent phase velocity and get amplified on the axial strain DAS seismograms, it is more difficult to detect the hidden deep Moon signals, which in contrast tend to have more energy on the current DAS insensitive off-axis. Thus, efforts to develop a space-qualified broadside-sensitive DAS are important, especially for imaging deep Moon structures.

It is also possible to combine DAS with other cable-based lunar programs to maximize the scientific returns. For example, it has been proposed to place a radio telescope on the far side of the Moon, which can avoid the radio noises from the Earth and detect the most sensitive radio signals from the universe. The idea of this telescope is to deploy a cable-linked antenna in a natural crater at the far side of the Moon (Hallinan et al., 2021). Thus, the fiber optic cables laid down could enable the deployment of both DAS and telescope with the minimum additional cost. Fiber deployment may be completed through several means. Artemis mission, astronauts may deploy the cable via crewed rovers (towed cable-plows are currently used to simultaneously trench and bury cables on Earth), or autonomous rovers may perform similar tasks. If a smaller lander is employed, such as with a Commercial Lunar Payload Service mission, fibers may be deployed across

the surface using small rockets or mortars. Although the cable tested in this study features a 1D linear geometry, more complex configurations, like a petal-shaped array, would be preferable for improved array performance. Expanding the 1D line array into a 2D network would offer additional resolution in the other direction, enhancing its ability to identify and retrieve seismic phases. In addition, these two facilities may also share other systems of power supply, environmental protection, and data processing/telemetry, which helps reduce cost further.

In conclusion, DAS can provide a cost-efficient solution for the future lunar dense seismic array deployment. Comparing to a sparse conventional seismic network (e.g., Apollo), a dense array enables us to detect more lunar seismic activities and overcome the challenges for improved deep Moon structure imaging. In this study, we compute lunar synthetic seismograms, which contain strong scattered waves due to small-scale heterogeneities in the top layer of the Moon, and demonstrate the advantage of DAS in retrieving the core reflected shear-wave ScS. For example, clear ScS can be retrieved from the scattered wave dominated seismograms by stacking data of a tens-of-kilometer-long DAS array when the heterogeneity velocity and density perturbations are up to 15 percent. Although only ScS is tested here, similar performances are expected for other deep mantle and core phases (e.g., core-reflected compressional-wave PcP and inner core reflected phase PKiKP). The advantages of DAS in seismicity detections and seismic structure imaging have been demonstrated in a number of experiments on the Earth, but more efforts and further evaluations are required to develop a space-proof DAS, which can undertake a long-term seismic monitoring task under the lunar environment conditions and record the extremely weak signals from small moonquakes.

### **Data and Resources**

The wave propagation numerical tool AxiSEM can be downloaded from http://seis.earth.ox.ac.uk/axisem/ (last accessed February 2024). The Apollo seismic waveform data used in this study can be obtained from the Incorporated Research Institutions for Seismology Data Management Center (IRIS-DMC) doi: 10.7914/SN/XA\_1969. The supplemental material contains signal-to-noise ratios (SNRs) of retrieved ScS with different cable lengths and channel numbers of distributed acoustic sensing (DAS) array. The supplemental material includes four supplement figures showing SNRs of retrieved ScS with different locations, cable lengths, and channel numbers of DAS array.

## **Declaration of Competing Interests**

The authors acknowledge that there are no conflicts of interest recorded.

#### **Acknowledgments**

The authors thank editors of *Seismological Research Letters* and two anonymous reviewers for their insightful suggestions and comments to improve the article. This work was supported by the Keck Institute for Space Studies study program. The authors acknowledge the use of the Generic Mapping Tools (GMT; Wessel *et al.*, 2013) software package.

#### References

- Araki, E., T. Yokobiki, H. Matsumoto, S. Baba, S. Tsuji, S. Nishida, Y. Machida, and Y. Tanaka (2022). Seafloor fiber optic sensing technological development to capture slow process in the Nankai trough megathrust, AGU Fall Meeting 2022, December 2022, San Francisco, California.
- Banerdt, W. B., S. E. Smrekar, D. Banfield, D. Giardini, M. Golombek, C. L. Johnson, P. Lognonné, A. Spiga, T. Spohn, C. Perrin, et al. (2020). Initial results from the InSight mission on Mars, Nature Geosci. 13, no. 3, 183–189, doi: 10.1038/s41561-020-0544-y.
- Blanchette-Guertin, J. F., C. L. Johnson, and J. F. Lawrence (2012). Investigation of scattering in lunar seismic coda, *J. Geophys. Res.* **117**, E06003, doi: 10.1029/2011JE004042.
- Blanchette-Guertin, J. F., C. L. Johnson, and J. F. Lawrence (2015). Effects of lateral variations in megaregolith thickness on predicted lunar seismic signals, *Geophys. Res. Lett.* **42**, 10–171, doi: 10.1002/2015GL066151.
- Canup, R. M., and E. Asphaug (2001). Origin of the Moon in a giant impact near the end of the Earth's formation, *Nature* **412**, 708–712, doi: 10.1038/35089010.
- Cheng, C. H., and M. N. Toksöz (1978). Tidal stresses in the Moon, *J. Geophys. Res.* **83**, 845–853, doi: 10.1029/JB083iB02p00845.
- Costa, L., H. F. Martins, S. Martín-López, M. R. Fernández-Ruiz, and M. González-Herráez (2019). Fully distributed optical fiber strain sensor with  $10-12\epsilon/\sqrt{}$  Hz sensitivity, *J. Lightwave Technol.* **37**, no. 18, 4487–4495, doi: 10.1109/JLT.2019.2904560.
- Dainty, A. M., M. N. Toksöz, K. R. Anderson, P. J. Pines, Y. Nakamura, and G. Latham (1974). Seismic scattering and shallow structure of the Moon in Oceanus Procellarum, *Moon* 9, 11–29, doi: 10.1007/BF00565388.
- Daubar, I., P. Lognonné, N. A. Teanby, K. Miljkovic, J. Stevanović, J. Vaubaillon, B. Kenda, T. Kawamura, J. Clinton, A. Lucas, et al. (2018). Impact-seismic investigations of the InSight mission. Space Sci. Rev. 214, 1–68, doi: 10.1007/s11214-018-0562-x.
- Frohlich, C., and Y. Nakamura (2009). The physical mechanisms of deep moonquakes and intermediate-depth earthquakes: How similar and how different? *Phys. Earth Planet. Inter.* **173**, 365–374, doi: 10.1016/j.pepi.2009.02.004.
- Gagnepain-Beyneix, J., P. Lognonné, H. Chenet, D. Lombardi, and T. Spohn (2006). A seismic model of the lunar mantle and constraints on temperature and mineralogy, *Phys. Earth Planet. Inter.* 159, no. 3–4, 140–166.
- Garcia, R. F., J. Gagnepain-Beyneix, S. Chevrot, and P. Lognonné (2011). Very preliminary reference Moon model, *Phys. Earth Planet. Inter.* 188, no. 1–2, 96–113.
- Garcia, R. F., A. Khan, M. Drilleau, L. Margerin, T. Kawamura, D. Sun, M. A. Wieczorek, A. Rivoldini, C. Nunn, and R. C. Weber, et al. (2019). Lunar seismology: An update on interior structure models, Space Sci. Rev. 215, 1–47.
- Gillet, K., L. Margerin, M. Calvet, and M. Monnereau (2017). Scattering attenuation profile of the Moon: Implications for shallow moon-quakes and the structure of the megaregolith, *Phys. Earth Planet. In.* **262**, 28–40, doi: 10.1016/j.pepi.2016.11.001.
- Goins, N. R., A. M. Dainty, and M. N. Toksoz (1981). Lunar seismology: The internal structure of the Moon, *J. Geophys. Res.* **86**, 5061–5074, doi: 10.1029/JB086iB06p05061.

- Hallinan, G., J. Burns, J. Lux, A. Romero-Wolf, L. Teitelbaum, T.-C. Chang, J. Kocz, J. Bowman, R. MacDowall, J. Kasper, et al. (2021). FARSIDE: A low radio frequency interferometric array on the lunar Farside, Bull. Am. Astron. Soc. 53, 379, doi: 10.3847/25c2cfeb.60683360.
- Haugland, S. M., J. Ritsema, P. E. van Keken, and T. Nissen-Meyer (2018). Analysis of PKP scattering using mantle mixing simulations and axisymmetric 3D waveforms, *Phys. Earth Planet. In.* 276, 226–233, doi: 10.1016/j.pepi.2017.04.001.
- Hood, L. L. (1986). Geophysical constraints on the lunar interior, in Origin of the Moon, W. K. Hartmann, R. J. Phillips, and G. J. Taylor (Editors), Lunar and Planetary Institute, Houston, 361–388.
- Hornman, J. C. (2017). Field trial of seismic recording using distributed acoustic sensing with broadside sensitive fibre-optic cables, *Geophys. Prospect.* **65**, 35–46, doi: 10.1111/1365-2478.12358.
- Jiang, X., Y. Wang, and T. Furumura (2015). Numerical simulation of lunar seismic coda caused by scattering in upper Moon crust, *Chin. J. Geophys.* 58, 1675–1691, doi: 10.6038/cjg20150519.
- Khan, A., J. A. Connolly, A. Pommier, and J. Noir (2014). Geophysical evidence for melt in the deep lunar interior and implications for lunar evolution. *J. Geophys. Res.* 119, no. 10, 2197–2221, doi: 10.1002/2014JE004661.
- Koyama, J., and Y. Nakamura (1980). Focal mechanism of deep moonquakes, *Lunar and Planetary Science Conference*, 17–21 March 1980, Houston, Texas, 1855–1865.
- Kuvshinov, B. N. (2016). Interaction of helically wound fibre-optic cables with plane seismic waves, *Geophys. Prospect.* **64**, 671–688, doi: 10.1111/1365-2478.12303.
- Lammlein, D. R. (1977). Lunar seismicity and tectonics, *Phys. Earth Planet. In.* **14**, 224–273, doi: 10.1016/0031-9201(77)90175-3.
- Laneuville, M., M. A. Wieczorek, D. Breuer, and N. Tosi (2013). Asymmetric thermal evolution of the Moon, *J. Geophys. Res.* **118**, no. 7, 1435–1452.
- Latham, G. V., M. Ewing, F. Press, G. Sutton, J. Dorman, Y. Nakamura, N. Toksöz, R. Wiggins, J. Derr, and F. Duennebier (1970). Passive seismic experiment, *Science* 167, 455–457, doi: 10.1126/science.167.3918.455.
- Li, Z., Z. Shen, Y. Yang, E. Williams, X. Wang, and Z. Zhan (2021). Rapid response to the 2019 Ridgecrest earthquake with distributed acoustic sensing, *AGU Adv.* **2**, e2021AV000395, doi: 10.1029/2021AV000395.
- Lim Chen Ning, I., and P. Sava (2018). Multicomponent distributed acoustic sensing: Concept and theory, *Geophysics* **83**, no. 2, P1–P8, doi: 10.1190/geo2017-0327.
- Lindsey, N. J., and E. R. Martin (2021). Fiber-optic seismology, *Annu. Rev. Earth Planet. Sci.* **49**, 309–336, doi: 10.1146/annurev-earth-072420-065213.
- Lindsey, N. J., T. C. Dawe, and J. B. Ajo-Franklin (2019). Illuminating seafloor faults and ocean dynamics with dark fiber distributed acoustic sensing, *Science* 366, 1103–1107, doi: 10.1126/science.aay5881.
- Lognonné, P., W. B. Banerdt, D. Giardini, W. T. Pike, U. Christensen, P. Laudet, S. De Raucourt, P. Zweifel, S. Calcutt, M. Bierwirth, et al. (2019). SEIS: Insight's seismic experiment for internal structure of Mars, Space Sci. Rev. 215, doi: 10.1007/s11214-018-0574-6.
- Lognonné, P., W. B. Banerdt, W. T. Pike, D. Giardini, U. Christensen, R. F. Garcia, T. Kawamura, S. Kedar, B. Knapmeyer-Endrun, L.

- Margerin, et al. (2020). Constraints on the shallow elastic and anelastic structure of Mars from InSight seismic data, *Nature Geosci.* **13**, 213–220, doi: 10.1038/s41561-020-0536-y.
- Lognonné, P., J. Gagnepain-Beyneix, and H. Chenet (2003). A new seismic model of the Moon: Implications for structure, thermal evolution and formation of the Moon, *Earth Planet. Sci. Lett.* **211,** 27–44, doi: 10.1016/S0012-821X(03)00172-9.
- Matsumoto, K., R. Yamada, F. Kikuchi, S. Kamata, Y. Ishihara, T. Iwata, H. Hanada, and S. Sasaki (2015). Internal structure of the Moon inferred from Apollo seismic data and selenodetic data from GRAIL and LLR, *Geophys. Res. Lett.* 42, 7351–7358, doi: 10.1002/2015GL065335.
- Nakamura, Y. (1977). Seismic energy transmission in an intensively scattering environment, *J. Geophys.* **43**, 389–399.
- Nakamura, Y. (1978). A1 moonquakes: Source distribution and mechanism, *Lunar and Planetary Science Conference*, 13–17 March 1978, Houston, Texas, 3589–3607.
- Nakamura, Y. (1983). Seismic velocity structure of the lunar mantle, *J. Geophys. Res.* **88**, 677–686, doi: 10.1029/JB088iB01p00677.
- Nakamura, Y. (2005). Farside deep moonquakes and the deep interior of the Moon, *J. Geophys. Res.* **110**, E0100, doi: 10.1029/2004JE002332.
- Nakamura, Y., and J. Koyama (1982). Seismic Q of the lunar upper mantle, *J. Geophys. Res.* **87**, 4855–4861, doi: 10.1029/JB087iB06p04855.
- Nakamura, Y., D. Lammlein, G. Latham, M. Ewing, J. Dorman, F. Press, and N. Toksoz (1973). New seismic data on the state of the deep lunar interior, *Science* 181, 49–51, doi: 10.1126/science.181.4094.49.
- Nakamura, Y., G. V. Latham, and H. J. Dorman (1982). Apollo lunar seismic experiment—Final summary, *J. Geophys. Res.* **87**, no. S01, A117–A123, doi: 10.1029/JB087iS01p0A117.
- Nissen-Meyer, T., M. van Driel, S. C. Stähler, K. Hosseini, S. Hempel, L. Auer, A. Colombi, and A. Fournier (2014). AxiSEM: Broadband 3-D seismic wavefields in axisymmetric media, *Solid Earth* 5, no. 1, 425–445, doi: 10.5194/se-5-425-2014.
- Nunn, C., R. F. Garcia, Y. Nakamura, A. G. Marusiak, T. Kawamura, D. Sun, L. Margerin, R. Weber, M. Drilleau, M. A. Wieczorek, et al. (2020). Lunar seismology: A data and instrumentation review, Space Sci. Rev. 216, 1–39, doi: 10.1007/s11214-020-00709-3.
- Nunn, C., W. T. Pike, I. M. Standley, S. B. Calcutt, S. Kedar, and M. P. Panning (2021). Standing on Apollo's shoulders: A microseismometer for the Moon, *Planet. Sci. J.* 2, no. 1, 36.
- Oberst, J., and Y. Nakamura (1991). A search for clustering among the meteoroid impacts detected by the Apollo lunar seismic network, *Icarus* **91**, 315–325, doi: 10.1016/0019-1035(91)90027-Q.
- Peterson, J. R. (1993). Observations and modeling of seismic background noise, U.S. Geol. Surv. Open-File Rep. 93-322, doi: 10.3133/ofr93322.
- Qin, C., A. C. Muirhead, and S. Zhong (2012). Correlation of deep moonquakes and mare basalts: Implications for lunar mantle structure and evolution, *Icarus* 220, 100–105, doi: 10.1016/j.icarus.2012.04.023.
- Rost, S., and C. Thomas (2002). Array seismology: Methods and applications, *Rev. Geophys.* **40**, 2-1–2-27, doi: 10.1029/2000RG000100.
- Sato, H., M. C. Fehler, and T. Maeda (2012). Seismic Wave Propagation and Scattering in the Heterogeneous Earth, Springer-Verlag Inc., New York.
- Spica, Z. J., M. Perton, E. R. Martin, G. C. Beroza, and B. Biondi (2020). Urban seismic site characterization by fiber-optic seismology, J. Geophys. Res. 125, no. 3, e2019JB018656.

- Sladen, A., D. Rivet, J. P. Ampuero, L. De Barros, Y. Hello, G. Calbris, and P. Lamare (2019). Distributed sensing of earthquakes and ocean-solid earth interactions on seafloor telecom cables, Nat. Commun. 10, 5777, doi: 10.1038/s41467-019-13793-z.
- Toksöz, M. N., A. M. Dainty, S. C. Solomon, and K. R. Anderson (1974). Structure of the moon, Rev. Geophys. 12, 539-567, doi: 10.1029/RG012i004p00539.
- Toksöz, M. N., N. R. Goins, and C. H. Cheng (1977). Moonquakes: Mechanisms and relation to tidal stresses, Science 196, 979-981, doi: 10.1126/science.196.4293.979.
- Vinnik, L., H. Chenet, J. Gagnepain-Beyneix, and P. Lognonne (2001). First seismic receiver functions on the Moon, Geophys. Res. Lett. 28, 3031-3034, doi: 10.1029/2001GL012859.
- Walter, F., D. Gräff, F. Lindner, P. Paitz, M. Köpfli, M. Chmiel, and A. Fichtner (2020). Distributed acoustic sensing of microseismic sources and wave propagation in glaciated terrain, Nat. Commun. 11, 1-10, doi: 10.1038/s41467-020-15824-6.
- Wang, Y., H. Takenaka, X. Jiang, and J. Lei (2013). Modelling two-dimensional global seismic wave propagation in a laterally heterogeneous whole-Moon model, Geophys. J. Int. 192, no. 3, 1271-1287, doi: 10.1093/gji/ggs094.
- Watters, T. R., R. C. Weber, G. C. Collins, I. J. Howley, N. C. Schmerr, and C. L. Johnson (2019). Shallow seismic activity and young thrust faults on the Moon, Nature Geosci. 12, 411-417, doi: 10.1038/s41561-019-0362-2.
- Weber, R. C., P. Lin, E. J. Garnero, Q. Williams, and P. Lognonné (2011). Seismic detection of the lunar core, Science 331, no. 6015, 309-312, doi: 10.1126/science.1199375.
- Wessel, P., W. H. F. Smith, R. Scharroo, J. Luis, and F. Wobbe (2013). Generic mapping tools: Improved version released, Eos Trans. AGU 94, no. 45, 409-410, doi: 10.1002/2013EO450001.
- Wieczorek, M. A., B. J. Jolliff, A. Khan, M. E. Pritchard, B. J. Weiss, J. G. Williams, L. L. Hood, K. Righter, C. R. Neal, C. K. Shearer, et al. (2006). The constitution and structure of the lunar interior, Rev. Mineral. Geochem. 60, 221-364, doi: 10.2138/rmg.2006.60.3.
- Wieczorek, M. A., G. A. Neumann, F. Nimmo, W. S. Kiefer, G. J. Taylor, H. J. Melosh, R. J. Phillips, S. C. Solomon, J. C. Andrews-Hanna, S.

- W. Asmar, et al. (2013). The crust of the Moon as seen by GRAIL, Science 339, 671-675, doi: 10.1126/science.1231530.
- Williams, E. F., M. R. Fernández-Ruiz, R. Magalhaes, R. Vanthillo, Z. Zhan, M. González-Herráez, and H. F. Martins (2019). Distributed sensing of microseisms and teleseisms with submarine dark fibers, Nat. Commun. 10, 5778, doi: 10.1038/s41467-019-13262-7.
- Wu, W., and J. C. Irving (2017). Using PKiKP coda to study heterogeneity in the top layer of the inner core's western hemisphere, Geophys. J. Int. 209, 672-687, doi: 10.1093/gji/ggx047.
- Wu, W., S. Ni, and J. C. Irving (2019). Inferring Earth's discontinuous chemical layering from the 660-kilometer boundary topography, Science 363, 736-740, doi: 10.1126/science.aav0822.
- Yamada, R., K. Matsumoto, F. Kikuchi, and S. Sasaki (2014). Error determination of lunar interior structure by lunar geodetic data on seismic restriction, Phys. Earth Planet. In. 231, 56-64, doi: 10.1016/j.pepi.2014.02.005.
- Yamada, R., I. Yamada, H. Shiraishi, S. Tanaka, Y. Takagi, N. Kobayashi, N. Takeuchi, Y. Ishihara, H. Murakami, and K. Yomogida, et al. (2009). Capability of the penetrator seismometer system for lunar seismic event observation, Planet. Space Sci. 57, no. 7, 751-763.
- Yao, Y. (2016). Imaging the mantle structure of the Earth and Moon from array based observations, Doctoral Dissertation, The University of Utah.
- Yu, C., Z. Zhan, N. J. Lindsey, J. B. Ajo-Franklin, and M. Robertson (2019). The potential of DAS in teleseismic studies: Insights from the Goldstone experiment, Geophys. Res. Lett. 46, 1320-1328, doi: 10.1029/2018GL081195.
- Zhan, Z. (2020). Distributed acoustic sensing turns fiber-optic cables into sensitive seismic antennas, Seismol. Res. Lett. 91, 1-15, doi: 10.1785/0220190112.

Manuscript received 28 February 2023 Published online 28 February 2024